ACS SENSORS

Article

Cite This: ACS Sens. 2019, 4, 2124−2130

pubs.acs.org/acssensors

Highly Sensitive Detection of Bladder Cancer-Related miRNA in Urine Using Time-Gated Luminescent Biochip

Yingqian Wang,[†,⊥] Zhihao Li,[†,⊥] Qiaosong Lin,[†,⊥] Yurong Wei,[†] Jie Wang,[†] Yingxue Li,[†] Ronghua Yang,[§] and Quan Yuan*[,†,‡]

[†]Key Laboratory of Analytical Chemistry for Biology and Medicine (Ministry of Education), College of Chemistry, Wuhan University, Wuhan 430072, China

[‡]Molecular Science and Biomedicine Laboratory, State Key Laboratory of Chemo/Biosensing and Chemometrics, College of Chemistry and Chemical Engineering, Hunan University, Changsha 410082, China

[§]School of Chemistry and Biological Engineering, Changsha University of Science and Technology, Changsha 410004, China

Supporting Information

ABSTRACT: Detection of biomarkers in complex samples is a significant health plan strategy for medical diagnosis, therapy monitoring, and health management. However, high background noise resulting from impurities and other analytes in complex samples has hampered the improvement of detection sensitivity and accuracy. Herein, an ultralow background biochip based on time-gated luminescent probes supported by photonic crystals (PCs) was successfully developed for detection of bladder cancer (BC)-related miRNA biomarkers with high sensitivity and specificity in urine samples. Coupled with the time-gated luminescence of long-lifetime luminescence probes and the luminescence-enhanced capability of PCs, the short-lived autofluorescence can be efficiently removed; thus, the detection sensitivity will be significantly improved. Benefiting from these merits, a detection limit of 26.3 fM is achieved. Furthermore, the biochip exhibits excellent performance in urinary miRNA detection, and good recoveries are also obtained. The developed biochip possesses unique properties of ultralow background and luminescence enhancement, thus offering a suitable tool for the detection of BC-related miRNA in urine. With rational design of probe sequences, the biochip holds great potential for many other biomarkers in real patient samples, making it valuable in areas such as medical diagnosis and disease evaluation.

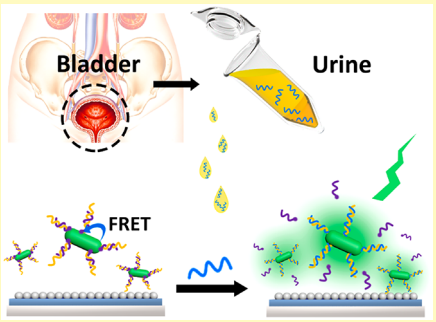

KEYWORDS: *long-lifetime luminescence, photonic crystals, miRNA detection, urine, autofluorescence*

Biomarker detection in complex samples plays an important role in early diagnosis, therapy evaluation, and healthcare.[1−6] However, a great number of impurities and other analytes exist in the complex samples, leading to high background signals.[7−9] For instance, urine and blood samples contain numerous proteins, nucleic acids, and small molecules.[10,11] Such complex components would result in nonspecific signals and lead to severe interference to the real target.[12,13] As a result, the detection sensitivity and accuracy of biomarkers in complex samples is limited.[14,15]

Fluorescence analysis has been widely recognized as one of the most powerful approaches for biosensing and biodetection.[16−18] For the detection in complex samples, impurities including proteins and small molecules would emit fluorescence when the fluorescent label is excited by a light source, leading to high background noise and severely hampering the improvement of detection sensitivity.[19,20] In this regard, it would be highly promising to develop an efficient strategy to eliminate the background fluorescence noise in complex samples.[21] Long-lifetime luminescence can still remain after removing the excitation.[22−24] Considering that the lifetime of most biological substances is below the nanosecond regime, the short-lived autofluorescence decays rapidly after cessation of excitation; however, the long-lifetime luminescence signals are still detectable.[24−28] Therefore, phosphors with long-lifetime luminescence are suitable candidates for eliminating autofluorescence in complex samples owing to their unique optical properties.[25−32]

Bladder cancer (BC), a kind of cancer arising from the tissues of the urinary bladder, is characterized by high morbidity, mortality, and cost, ranking second among the various genitourinary cancers.[33,34] Detection of cancer-related miRNAs in patient urine opens up a new avenue in noninvasive and painless diagnosis of BC.[35,36] Herein, we establish an optical biochip with enhanced luminescence signals and ultralow background fluorescence interference based on photonic crystals (PCs)-supported long-lifetime luminescence probes for BC-related miRNA-21 (miR-21) detection in urine, based on the principle of hybridization. Previous studies have demonstrated that PCs, a dielectric

Received: May 21, 2019
Accepted: July 17, 2019
Published: July 17, 2019

DOI: 10.1021/acssensors.9b00927
ACS Sens. 2019, 4, 2124−2130

periodic material, can reflect light in certain wavelength ranges and then amplify detecting signals, thus increasing the detection sensitivity.[37−39] As shown in Scheme 1, single-

Scheme 1. Schematic Illustration of Time-Gated Detection by the Developed Biochip

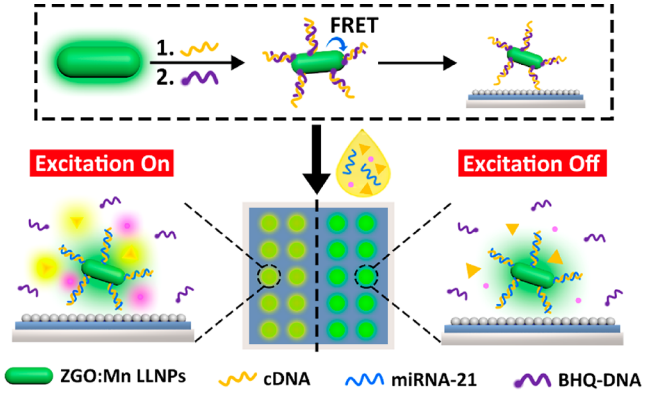

stranded DNAs (denoted as cDNAs) that are fully complementary to miR-21 are functionalized on long-lifetime luminescence nanoparticles (LLNPs) and further partially hybridized with black-hole-quencher-labeled DNAs (BHQ-DNAs). The luminescence can be quenched through FRET between the LLNPs and BHQ dyes. After addition of miR-21, the longer sequence of the target makes it more competitive toward to the cDNAs, thus leading to the detachment of BHQ-DNAs from the cDNAs. Consequently, the long-lifetime luminescence of LLNPs is restored. Our designed biochip can realize target miR-21-triggered luminescence "off−on" transformation; meanwhile, the luminescence signals are enhanced by PCs to improve the detection sensitivity. Additionally, when the excitation is turned off, the long-lifetime luminescence probes can remain luminescent, whereas the autofluorescence originating from the coexcited biomolecules decays rapidly, significantly decreasing the background signals. Therefore, this biochip features amplified luminescence signal outputs combined with ultralow background interference, which endows the biochip with significantly improved sensitivity for urine miR-21 detection. To the best of our knowledge, this is the first report in which an external excitation-free luminescence probe is coupled to an amplifier-like PCs substrate for miRNA detection in real urine samples. The biochip exhibits high sensitivity and low background for the analysis of urinary miRNA, providing a novel insight for BC diagnosis. Furthermore, rational design of the probe sequences enables our biochip to detect many other pivotal biomarkers, putting forward a new pathway to the applications of medical diagnosis and health assessment.

EXPERIMENTAL SECTION

Materials. Zinc nitrate hexahydrate ($Zn(NO_3)_2·6H_2O$), germanium oxide (GeO_2, 99.99%), manganese nitrate ($Mn(NO_3)_2$), 1-ethyl-3-[3-dimethyllamino-propyl]carbodiimide hydrochloride (EDC), 3-aminopropyltriethoxysilane (APTES), tris(hydroxymethyl)-aminomethane hydrochloride (Tris-HCl), 4-(2-hydroxyethyl)-1-piperazineethanesulfonic acid (HEPES), 4-(*N*-maleimidomethyl)-cyclohexane-1-carboxylic acid 3-sulfo-*N*-hydroxysuccinimide ester sodium salt (Sulfo-SMCC), and *N*-hydroxysuccinimide (NHS) were obtained from Aladdin. Sodium hydroxide (NaOH), concentrated nitric acid (HNO_3), ammonium hydroxide ($NH_3·H_2O$), and *N*,*N*-dimethylformamide (DMF, C_3H_7NO) were obtained from Sinopharm Chemical Reagent Co. (China). Monodispersed latex spheres polystyrene (PS, m/v = 5%) was obtained from Huge Biotechnology. PDMS (Sylgard 184 silicone elastomer kit, Dow) and curing agent were purchased from Dow Corning.

Nucleotide Sequences. All the nucleotides were purchased from NingBo Karebay Biochem Co., Ltd. The sequences of involved nucleotides are as follows:

Complementary nucleotides of miR-21 (named cDNA): 5′-NH_2-T CAA CAT CAG TCT GAT AAG CTA TTT TTT TTT-SH-3′.

BHQ-DNA: 5′-BHQ-1-TAG CTT ATC AGA CT-3′.

miR-21 (used in buffer): 5′-TAG CTT ATC AGA CTG ATG TTG A-3′.

miR-21 (used in urine): 5′-UAG CUU AUC AGA CUG AUG UUG A-3′.

Single mismatched miR-21 (named SM miR-21): 5′-TAG **G**TT ATC AGA CTG ATG TTG A-3′.

Double mismatched miR-21 (named DM miR-21): 5′-TAG **G**TT ATC AGA CTG AT**A** TTG A-3′.

Triple mismatched miR-21 (named TM miR-21): 5′-TAG **G**TT ATC **T**GA CTG AT**A** TTG A-3′.

Apparatus. The shape and size of the LLNPs was characterized by a transmission electron microscope (200 kV, JEOL, JEM-2100, Japan). Energy dispersive X-ray (EDX) analysis of the LLNPs was also conducted during TEM measurements. Zeta potential was measured by a Malvern Zetasizer Nano ZS system. The crystal structure was measured on a Bruker X-ray diffractometer with Cu Kα radiation (λ = 1.5406 Å) (Bruker, D8 Advance, Germany). The decay images were conducted on an IVIS Lumina XR Imaging System (Caliper, America). The morphology of PC substrate was characterized by field emission electron microscopy (Zeiss Merlin Compact, England). The photoluminescence spectra and long-lifetime luminescence spectra were recorded on a fluorescence spectrometer (Hitachi, F4600, Japan). The photoluminescence and long-lifetime luminescence images were obtained by a digital camera (Nikon, D3000, Japan). A commercial ZF5 portable UV lamp was used as excitation source.

Synthesis of Zn_2GeO_4:Mn (ZGO:Mn) LLNPs. The ZGO:Mn LLNPs were prepared according to the previous reports.[26,28] In brief, $Zn(NO_3)_2$ (2 mmol) and $Mn(NO_3)_2$ (0.005 mmol) were dissolved into 11 mL of deionized water and then 300 μL of HNO_3 was added under vigorous stirring. GeO_2 powder was dissolved in 2 mol L^{-1} NaOH solution to obtain a clear Na_2GeO_3 solution. Then, Na_2GeO_3 (1 mmol) was added drop by drop into the above solution, followed by immediate addition of ammonium hydroxide (28%, wt) to adjust the pH value of the mixture to 9.5. After stirring at room temperature for 1 h, the mixture was then transferred to a 20 mL Teflon-lined autoclave and reacted at 220 °C for 10 h. The hydrophilic products could be obtained after centrifugation and washing several times with water.

Measurement of the Decay Images of ZGO:Mn LLNPs. 0.1 g of the ZGO:Mn LLNPs were placed into a 48-well plate and the plate was placed into the IVIS Lumina XR Imaging System. A portable UV lamp was used to illuminate the LLNPs for 3 min. After that, the door of the Imaging System was immediately closed and the decay images at different times were collected.

Synthesis of cDNA-Functionalized ZGO:Mn LLNPs (ZGO:Mn-cDNA). The prepared ZGO:Mn LLNPs were modified with an amino group (denoted as ZGO:Mn-NH_2) first. Briefly, 25 mg of ZGO:Mn LLNPs was added into 10 mL of DMF under ultrasonic waves and then vigorously stirred, followed by addition of 100 μL of APTES drop by drop. The resulting mixture was heated to 80 °C and maintained at the temperature for 12 h. The products were obtained after centrifugation and washed several times with DMF. Then, the obtained ZGO:Mn-NH_2 LLNPs were resuspended in deionized water for further use. Next, the ZGO:Mn-NH_2 LLNPs were functionalized with cDNA according to a previous protocol. Typically, 0.4 mg of Sulfo-SMCC was dissolved into 200 μL of HEPES buffer solution (10 mM, pH 7.2) and then mixed with 800 μL of HEPES buffer solution containing 1 mg of ZGO:Mn-NH_2 LLNPs. After incubation at 25 °C for 2 h, the activated LLNPs were obtained after centrifugation and

DOI: 10.1021/acssensors.9b00927
ACS Sens. 2019, 4, 2124−2130

washing several times with HEPES buffer, followed by resuspending into 1 mL of HEPES buffer. Then, 2 nmol of cDNA was mixed with the above solution and incubated at 25 °C overnight. Excess cDNA was removed by centrifugation and washing with deionized water. The cDNA modified LLNPs were resuspended in 1 mL of Tris-HCl buffer solution and stored at 4 °C.

Preparation of miRNA Probe (Denoted as ZGO:Mn-probe). 0.6 nmol of BHQ-DNA was added into the above Tris-HCl buffer solution containing 1 mg mL^{-1} of ZGO:Mn-cDNA and then incubated at 37 °C for 3 h under shaking. The obtained product was collected after centrifugation and washing with Tris-HCl buffer several times. After that, the ZGO:Mn-probe was resuspended in 1 mL of Tris-HCl buffer solution and stored at 4 °C for further use.

Fabrication of PCs Substrate. Solvent evaporation was applied to fabricate the PCs substrate. In brief, PDMS and the curing agent (10:1 m/m) were mixed together under vigorous stirring. After that, the mixture was treated under vacuum until no bubbles emerged. Then, the mixture was spin-coated on the cover glass (3000 rpm min^{-1}, 30 s) and precured at 60 °C overnight. Next, 3 μL of polystyrene (PS) colloid suspension (2 wt %) was dropped vertically on the PDMS-coated glass and dried on a heating plate at 40 °C.

Measurement of Long-lifetime Luminescence of LLNPs on Different Substrates. 3 μL of LLNPs solution (1.0 mg mL^{-1}) was dropped on a PDMS substrate and PCs substrate, respectively. After that, the substrates were treated on the heating plate at 40 °C until the droplets were dry. The long-lifetime luminescence of LLNPs on different substrates was measured on a fluorescence spectrometer with the excitation of 269 nm.

Detection of miR-21 in Buffer Using PCs-Based Sensing Biochip. The ZGO:Mn-probe was first linked to the PCs substrate by reacting with EDC and NHS. In brief, EDC (0.5 mg) and NHS (1 mg) were dissolved in 1 mL of ultrapure water. After that, 3 μL of the resulting solution that serves as the activator was dropped onto the PC substrates, followed by incubating at 37 °C for 10 min. After washing three times with ultrapure water, the activated PCs substrate was obtained. Then, 3 μL of the ZGO:Mn-probe solution (1 mg mL^{-1}) was dropped onto the PCs substrate and incubated at the same temperature for another 30 min. Next, the unlinked ZGO:Mn-probe was washed away by PB buffer solution (pH 7.0, 10 mM), and then, 3 μL of the standard miR-21 solution with different concentrations was added onto the PCs substrate and reacted at 37 °C for 2 h. After washing with ultrapure water three times and drying, the long-lifetime luminescence spectra were measured using the fluorescence spectrometer.

Detection of miR-21 in Urine on the PCs Substrate. The viability of the PC-based biochip for miR-21 detection in urine samples was performed using fresh urine spiked with the target. The urine was collected from three healthy volunteers. Then, different amounts of miR-21 were directly added to the 10-fold dilution of urine samples. The detection was similar to the above-mentioned approach, except for the washing step with urine rather than buffer solution.

RESULTS AND DISCUSSION

Characterization of the ZGO:Mn LLNPs. Transmission electron microscopy (TEM) was used to characterize the shape of ZGO:Mn LLNPs. As shown in Figure 1a and Figures S1−S2, the LLNPs display well-defined monodisperse nanorod shapes with average length of about 55 nm. Well-resolved lattice fringes also can be observed from high-resolution TEM (HRTEM) images, confirming the formation of well-crystallized ZGO:Mn crystal (Figure S3). X-ray powder diffraction (XRD) was further utilized to characterize the crystal structure of ZGO:Mn LLNPs (Figure S4). It can be observed that the XRD pattern is well-matched to the standard card [JCPDS No. 11-0687], indicating the crystallization of the rhombohedral phase of Zn_2GeO_4. Energy dispersive X-ray analysis further

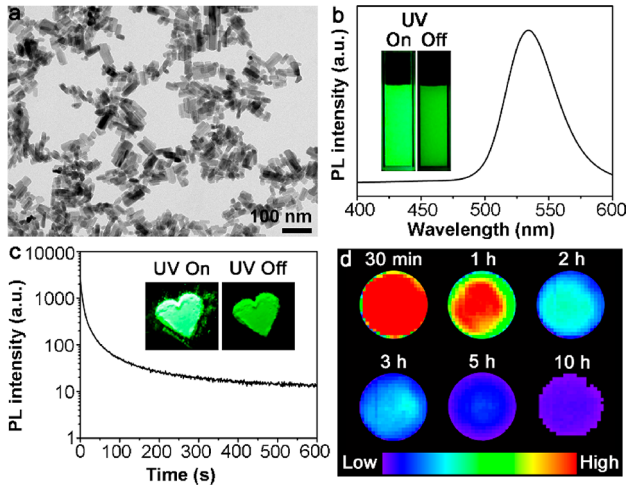

Figure 1. (a) TEM image of ZGO:Mn LLNPs. (b) Photoluminescence spectrum of the ZGO:Mn LLNPs. Inset: visible luminescence photograph of ZGO:Mn solution under UV illumination and after removing UV illumination. (c) Luminescence decay curve of ZGO:Mn LLNPs. Inset: visible luminescence photograph of ZGO:Mn powder. (d) Luminescence decay images of ZGO:Mn LLNPs.

confirms the presence of all four elements in the obtained LLNPs (Figure S5).

The luminescence properties of ZGO:Mn LLNPs were further investigated. Following UV excitation at 269 nm by a built-in xenon lamp within the fluorescence spectrophotometer, an extremely strong green emission band at around 535 nm can be observed (Figure 1b). The inset image in Figure 1b illustrates that ZGO:Mn LLNPs show visible green long-lifetime luminescence after removing UV excitation by a portable 254 nm UV lamp. Figure 1c shows the long-lifetime luminescence decay curve of ZGO:Mn LLNPs monitored at 535 nm after illumination by a UV lamp for 20 min. It can be observed that ZGO:Mn LLNPs display distinct long-lifetime luminescence with a decay time longer than 600 s, confirming the successful synthesis of ZGO:Mn LLNPs. Furthermore, the visualized decay images of ZGO:Mn LLNPs were further collected. As shown in Figure 1d, the long-lifetime luminescence signals are still detectable even after 10 h of decay.

PCs-Based Enhancement Effect of Long-Lifetime Luminescence. PCs are characterized by highly ordered nanostructure with the ability to manipulate light and enhance spontaneous emission. Here, PCs are chosen as a promising candidate to realize the enhancement of long-lifetime luminescence. The schematic illustration of the fabrication of PCs substrate is shown in Figure S6. Specifically, the droplets containing monodispersed carboxyl-modified polystyrene (PS) nanospheres are first dropped onto a hydrophobic PDMS substrate. Next, water evaporation can induce self-assembly of PS nanospheres, leading to the formation of a PCs substrate. The long-lifetime luminescence of ZGO:Mn LLNPs deposited on the substrate with or without PCs is illustrated in Figure 2a. Without PCs, luminescence can easily penetrate through the PDMS-coated glass, leading to the decrease of reflected luminescence that will be detected as the luminescence signals by the detector, whereas with PCs, the transmitted light is obviously prevented and the reflected luminescence is further enhanced, thus improving the detection signals. The TEM

DOI: 10.1021/acssensors.9b00927
ACS Sens. 2019, 4, 2124−2130

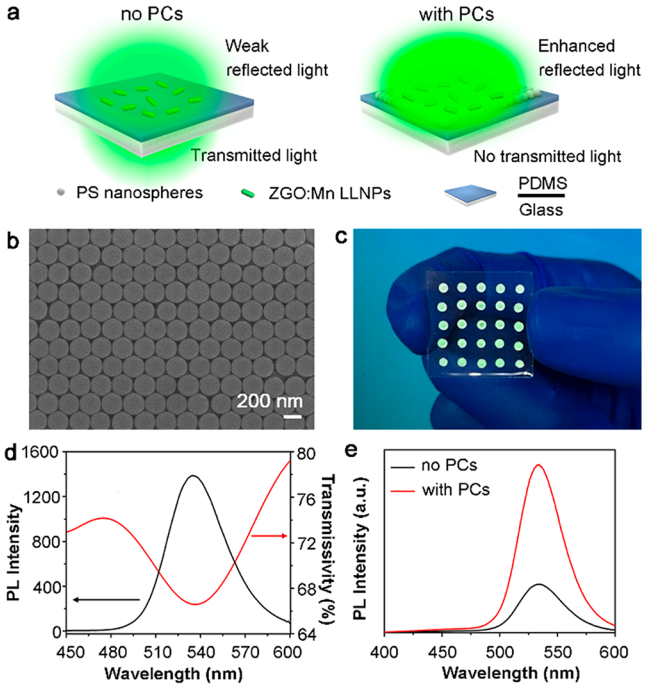

Figure 2. (a) Diagram of long-lifetime luminescence of ZGO:Mn LLNPs deposited on the substrate with or without PCs. (b) SEM image of PC substrate. (c) Photograph of the PC substrate after exposure to sunlight. (d) Transmittance spectrum of the PCs together with the long-lifetime luminescence spectrum of ZGO:Mn. (e) Long-lifetime luminescence spectra of ZGO:Mn on different substrates.

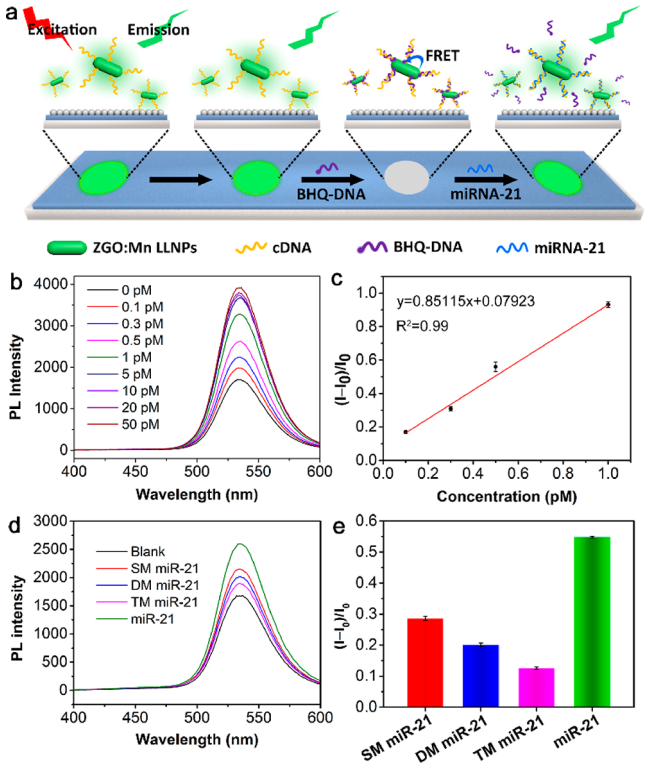

Figure 3. (a) Illustration of miR-21 detection by the biochip. (b) Long-lifetime luminescence recovery of the sensing biochip in the presence of different concentrations of miR-21 within the range of 0.1−50.0 pM. (c) Linear relationship between the long-lifetime luminescence recovery and the concentration of target miR-21 ranging from 0.1 pM to 1 pM. (d) Long-lifetime luminescence spectrum after adding miR-21 and 100-fold concentration of single-mismatched miR-21 (denoted as SM miR-21), double-mismatched miR-21 (denoted as DM miR-21), and triple-mismatched miR-21 (denoted as TM miR-21), respectively. Buffer was used as the control. (e) Histogram of luminescence varieties corresponding to part d. Data are means ± s.d. (n = 3).

images confirm that PS nanospheres are well-monodispersed in water (Figure S7). The surface morphology of the PC substrate assembled by the PS nanospheres was characterized by scanning electron microscope (SEM). PS nanospheres with average diameters of 230 nm are close-packed and arranged in the ordered face-centered cubic structure (Figure 2b and Figure S8). Due to the Bragg scattering effect, the PCs substrate possesses a brilliant green reflected light under sunlight (Figure 2c). The transmission band of PC substrate is peaking at about 535 nm, which is well overlapped with the emission band of long-lifetime luminescence that is centered at 535 nm, indicating that PCs can efficiently reflect luminescence (Figure 2d). The intensity of long-lifetime luminescence of ZGO:Mn supported with and without PC substrate was further measured. It can be observed that 3-fold enhancement of long-lifetime luminescence after addition of PC substrate is realized (Figure 2e). The LLNPs supported with the PCs substrate exhibits higher luminescence intensity at the same measured time compared with those without PCs (Figure S9). To further investigate the luminescence of LLNPs with or without the PCs substrate, the luminescence decay of LLNPs was further monitored by an IVIS Lumina XR Imaging System. As shown in Figure S10, LLNPs with PCs exhibit a higher intensity than those without PCs. The above results clearly prove that the PCs substrate can serve as an efficient amplifier for enhancing the long-lifetime luminescence of ZGO:Mn LLNPs.

Characterization of Stability of the Detection Biochip. The detection biochip is based on the target-triggered long-lifetime luminescence off−on principle (Figure 3a). Owing to the good overlap between the absorption band of BHQ and the long-lifetime luminescence spectrum of LLNPs, BHQ can efficiently quench the luminescence of the LLNPs-based detection probe. The prepared ZGO:Mn LLNPs were modified with an amino group (denoted as ZGO:Mn-NH_2) first and then modified with DNA. The changes of zeta potential values of nanoparticles confirm that c-DNA was successfully modified on the ZGO:Mn-NH_2 LLNPs (Figure S11). Then, different concentrations of BHQ-DNA were employed to investigate the luminescence quenching of ZGO:Mn-cDNA. As expected, the long-lifetime luminescence intensity of ZGO:Mn-cDNA gradually decreases with addition of increasing amounts of BHQ-DNA. Specifically, the luminescence quenching percentage reaches the maximum when 0.6 μM of BHQ-DNA was mixed with 1 mg mL^{-1} of ZGO:Mn-cDNA (Figure S12). Additionally, the quenching time is also optimized; the intensity of long-lifetime luminescence almost remains unchanged after 3 h of adding BHQ-DNA (Figure S13).

Considering that the sensing interfaces are vital for the detection performance,[40] the uniformity and stability of sensing interfaces were investigated. SEM was first used to characterize the sensing interfaces. As shown in Figure S14a−e, PCs substrates were uniformly covered by several layers of luminescent probes in different batches of biochips. After storing at room temperature for 14 days, the surface of the

DOI: 10.1021/acssensors.9b00927
ACS Sens. 2019, 4, 2124−2130

biochip is not changed (Figure S14f). Furthermore, contact angle measurement was applied to study the sensing interfaces of biochips. We have fabricated several different batches of biochips and the contact angle was measured. As shown in Figure S15a−c, all the biochips display highly hydrophilic behavior with a contact angle of 40.1 ± 1.05°. After storing at room temperature for 14 days, the contact angle of 39.7 ± 0.9° was observed, which is similar to the original contact angle (Figure S15d−f). The above results further confirm the formation of uniform and stable sensing interfaces.

Next, the tolerance of the biochip to preserve time, humidity, and nuclease was studied. The initial luminescence intensity of the biochips that have been stored at room temperature for different days was measured. As shown in Figure S16a, the luminescence intensity is nearly consistent with the prolonged time, demonstrating the long-term stability of the biochips. In addition, the stability of the biochip at different humidity levels was also investigated. The biochips were placed at room temperature but different humidity for 24 h, and then the luminescence intensity was measured. As shown in Figure S16b, the luminescence intensity of biochips is not changed, confirming that a high humidity will not damage the stability of the biochips. Taken together, the sensing biochips are stable enough to be preserved for a long time even at a high humidity. However, the luminescence intensity gradually increased by small degrees when the biochip was treated with nuclease, indicating that the FRET between BHQ and the long-lifetime nanoparticles was destroyed due to the degradation of DNA by nuclease, and then the luminescence was recovered (Figure S17).

Investigation of the Sensitivity and Selectivity of Detection Biochip. Different concentrations of miR-21 in buffer solution were further assayed. In our experiments, three repeats are used for the data. As shown in Figure 3b, the intensity of long-lifetime luminescence is gradually recovered with an increasing amount of the target. A linear relationship between the long-lifetime luminescence recovery and the concentration of target miR-21 within the range of 0.1−1 pM is obtained (Figure 3c). According to the $3s/\sigma$ criterion (s, standard deviation of 11 blank samples; σ, slope of the linear work curve), the limit of detection (LOD) of miR-21 is calculated as 26.3 fM. Compared to most previous reports, our method exhibits a lower LOD (Table S1). Additionally, low standard deviation can be observed from the calibration curve, indicating good precision of the as-built detection biochip. In additional, single-mismatched miR-21 (denoted as SM miR-21), double-mismatched miR-21 (denoted as DM miR-21), and triple-mismatched miR-21 (denoted as TM miR-21) were employed to investigated the specificity of the sensing biochip. The long-lifetime luminescence signal decreases with the increasing number of mismatches; however, all three kinds of mismatched sequences with 100 times higher concentration of the target miR-21 only induce less change of the long-lifetime luminescence intensity, suggesting that the proposed method also exhibits high selectivity for target miR-21 over some other mismatched sequences (Figure 3d,e). Two hours are required for hybridization in our experiment. It would be better if the reaction time could be shortened for some specific conditions and applications.

MiR-21 Detection in Urine Samples. Considering that abnormal expression of miRNA in urine is related to the development of BC, miRNA detection in urine is of great importance for noninvasive and painless diagnosis of BC. The detection of miR-21 in human urine is illustrated in Figure 4a. An appropriate amount of miR-21 was spiked into urine, and

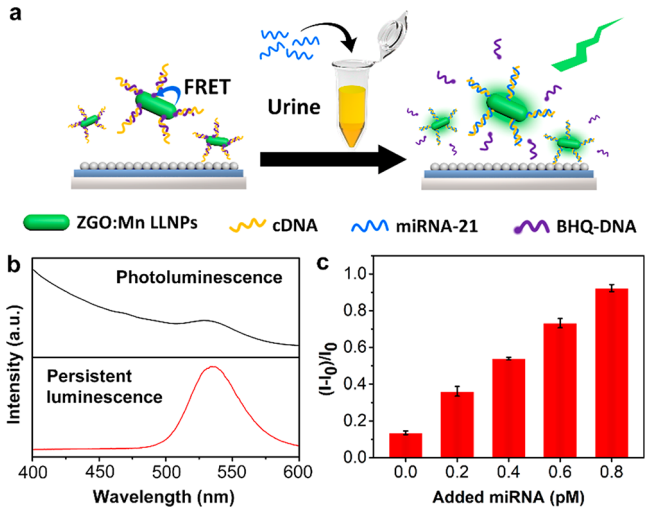

Figure 4. (a) Illustration of miR-21 detection in human urine by the developed biochip. (b) Photoluminescence and long-lifetime luminescence spectra of human urine containing ZGO:Mn-cDNA. (c) Recovery of long-lifetime luminescence after spiking different concentrations of miR-21 into urine. Data are means ± s.d. (n = 3).

then the above sample was employed to trigger the recovery of long-lifetime luminescence. Human urine contains substantial organic compounds that may be co-excited under light excitation, thus resulting in background fluorescence interference and decreasing detection sensitivity. As shown in Figure 4b, 10-fold dilution of fresh urine containing 1 mg mL^{-1} ZGO:Mn-cDNA displays obvious autofluorescence signals in the range of 400−600 nm under the photoluminescence mode with excitation wavelength of 269 nm, and the luminescence signals of ZGO:Mn-cDNA cannot be distinguished from the autofluorescence interference. However, after removing the excitation light, the autofluorescence signals disappear quickly, and the long-lifetime luminescence signals can be clearly observed, confirming that long-lifetime luminescence nanomaterials offer great potential in eliminating autofluorescence. We also measured the luminescence intensity of the probe under the excitation of different wavelengths. As presented in Figure S18a, the luminescence intensity of the probes is related to the wavelength of excitation light. Although the excitation wavelength has an effect on the intensity of the probes, it can be clearly observed from Figure S18b that all of the luminescent probes exhibit strong emission at 535 nm without the interference of background fluorescence under the excitation of different wavelengths, indicating that all wavelengths within the range of 255−320 nm can be selected to excite the probe for the background-free detection. Ten-fold dilution of urine was necessary to ensure that the concentration of miR-21 was in the linear range and to obtain quantitative recovery of the spiked miR-21.

Next, human urine spiked with various concentrations of miR-21 was employed to test the detection capability in such complicated matrix. With the increasing concentration of miR-21, the corresponding long-lifetime luminescence shows upward trends (Figure 4c). Additionally, the recovery of spiked miR-21 was also investigated and the obtained concentrations of miR-21 in urine are listed in Table 1. The

DOI: 10.1021/acssensors.9b00927
ACS Sens. 2019, 4, 2124−2130

Table 1. Recovery (%) (Means ± s.d., n = 3) of Spiked miR-21 with Different Concentrations in 10-Fold Diluted Urine

Sample	Determined miR-21 (10^{-14} M)	Added miR-21 (10^{-14} M)	miR-21 found (10^{-14} M)	Recovery (%)	RSD (%,n = 3)
Urine-1	13.56 ± 0.97	20.00	36.12 ± 2.58	107.79	10.11
Urine-1	13.56 ± 0.97	40.00	53.86 ± 0.72	100.57	1.16
Urine-1	13.56 ± 0.97	50.00	65.75 ± 1.66	103.45	2.51
Urine-1	13.56 ± 0.97	60.00	73.20 ± 2.52	99.50	2.82
Urine-1	13.56 ± 0.97	80.00	92.30 ± 1.95	98.64	1.31
Urine-2	20.14 ± 1.84	50.00	74.74 ± 1.80	106.56	1.18
Urine-3	33.34 ± 1.42	50.00	85.82 ± 3.08	102.96	1.95

good recoveries ranging from 97.33% to 117.9% of known amounts of miR-21 in the urine samples definitely demonstrated the reliability of our detection biochip for detecting miRNAs in complex biological matrix.

CONCLUSION

In conclusion, we have highlighted an ultralow background sensing biochip based on the long-lifetime luminescence probe supported by PCs substrate for miR-21 detection in human urine. Benefiting from the long-lived luminescence of the long-lifetime luminescence probe, autofluorescence from the complicated biological matrix can be efficiently eliminated after removing the excitation source. Coupled to the luminescence enhancement ability of the PCs substrate, our proposed biochip shows enhanced detection performance. Based on these merits, high sensitivity and good specificity are realized in quantitative detection of target miR-21 in a buffer solution. Additionally, the sensing biochip also exhibits excellent applicability to complicated human urine. With a simple but flexible configuration of the detection biochip, the design possesses great potential as a versatile strategy for the detection of many other targets. We further anticipate that this strategy will produce tremendous opportunities not only for noninvasive BC diagnosis but also for the evaluation of other significant diseases.

ASSOCIATED CONTENT

Supporting Information

The Supporting Information is available free of charge on the ACS Publications website at DOI: 10.1021/acssensors.9b00927.

TEM, HRTEM, and SEM imaging; Statistical analysis of the size of ZGO:Mn LLNPs by TEM; XRD patterns; EDX analysis; Illustration of fabrication of PC substrate; Luminescence decay; Contact angles; Comparison of our methods to other previously reported assays (table) (PDF)

AUTHOR INFORMATION

Corresponding Author

*E-mail: yuanquan@whu.edu.cn.

ORCID

Jie Wang: 0000-0003-4170-8470

Ronghua Yang: 0000-0001-7873-6892

Quan Yuan: 0000-0002-3085-431X

Author Contributions

⊥Yingqian Wang, Zhihao Li, and Qiaosong Lin contributed equally.

Notes

The authors declare no competing financial interest.

ACKNOWLEDGMENTS

This work was supported by the National Key R&D Program of China (2017YFA0208000, 2016YFF0100800), National Natural Science Foundation of China (21675120), National Postdoctoral Program for Innovative Talents (BX20180223), National Basic Research Program of China (973 Program, Grants 2015CB932600), Ten Thousand Talents Program for Young Talents. Q. Yuan thanks the large-scale instrument and equipment sharing foundation of Wuhan University.

REFERENCES

(1) Nakamura, A.; Kaneko, N.; Villemagne, V. L.; Kato, T.; Doecke, J.; Doré, V.; Fowler, C.; Li, Q.-X.; Martins, R.; Rowe, C.; Tomita, T.; Matsuzaki, K.; Ishii, K.; Ishii, K.; Arahata, Y.; Iwamoto, S.; Ito, K.; Tanaka, K.; Masters, C. L.; Yanagisawa, K. High Performance Plasma Amyloid-β Biomarkers for Alzheimer's Disease. *Nature* **2018**, *554*, 249−254.

(2) Monroe, M. R.; Daaboul, G. G.; Tuysuzoglu, A.; Lopez, C. A.; Little, F. F.; Ünlü, M. S. Single Nanoparticle Detection for Multiplexed Protein Diagnostics with Attomolar Sensitivity in Serum and Unprocessed Whole Blood. *Anal. Chem.* **2013**, *85*, 3698−3706.

(3) Stewart, A. J.; Hendry, J.; Dennany, L. Whole Blood Electrochemiluminescent Detection of Dopamine. *Anal. Chem.* **2015**, *87*, 11847−11853.

(4) Kobayashi, H.; Ogawa, M.; Alford, R.; Choyke, P. L.; Urano, Y. New Strategies for Fluorescent Probe Design in Medical Diagnostic Imaging. *Chem. Rev.* **2010**, *110*, 2620−2640.

(5) Weissleder, R. A Clearer Vision for in Vivo Imaging. *Nat. Biotechnol.* **2001**, *19*, 316−317.

(6) Min, X.; Zhuang, Y.; Zhang, Z.; Jia, Y.; Hakeem, A.; Zheng, F.; Cheng, Y.; Tang, B. Z.; Lou, X.; Xia, F. Lab in a Tube: Sensitive Detection of MicroRNAs in Urine Samples from Bladder Cancer Patients Using a Single-Label DNA Probe with AIEgens. *ACS Appl. Mater. Interfaces* **2015**, *7*, 16813−16818.

(7) Duan, R.; Zhang, Z.; Zheng, F.; Wang, L.; Guo, J.; Zhang, T.; Dai, X.; Zhang, S.; Yang, D.; Kuang, R.; Wang, G.; He, C.; Hakeem, A.; Shu, C.; Yin, P.; Lou, X.; Zeng, F.; Liang, H.; Xia, F. Combining Protein and miRNA Quantification for Bladder Cancer Analysis. *ACS Appl. Mater. Interfaces* **2017**, *9*, 23420−23427.

(8) Sparks, H.; Kondo, H.; Hooper, S.; Munro, I.; Kennedy, G.; Dunsby, C.; French, P.; Sahai, E. Heterogeneity in Tumor Chromatin-doxorubicin Binding Revealed by in Vivo Fluorescence Lifetime Imaging Confocal Endomicroscopy. *Nat. Commun.* **2018**, *9*, 2662.

(9) Lou, X.; Zhuang, Y.; Zuo, X.; Jia, Y.; Hong, Y.; Min, X.; Zhang, Z.; Xu, X.; Liu, N.; Xia, F.; Tang, B. Z. Real-Time, Quantitative Lighting-up Detection of Telomerase in Urines of Bladder Cancer Patients by AIEgens. *Anal. Chem.* **2015**, *87*, 6822−6827.

(10) Zhuang, Y.; Zhang, M.; Chen, B.; Duan, R.; Min, X.; Zhang, Z.; Zheng, F.; Liang, H.; Zhao, Z.; Lou, X.; Xia, F. Quencher Group Induced High Specificity Detection of Telomerase in Clear and Bloody Urines by AIEgens. *Anal. Chem.* **2015**, *87*, 9487−9493.

(11) Duan, R.; Wang, B.; Zhang, T.; Zhang, Z.; Xu, S.; Chen, Z.; Lou, X.; Xia, F. Sensitive and Bidirectional Detection of Urine Telomerase Based on the Four Detection-Color States of Difunctional Gold Nanoparticle Probe. *Anal. Chem.* **2014**, *86*, 9781−9785.

DOI: 10.1021/acssensors.9b00927
ACS Sens. 2019, 4, 2124−2130

(12) Galievsky, V. A.; Stasheuski, A. S.; Krylov, S. N. Improvement of LOD in Fluorescence Detection with Spectrally Nonuniform Background by Optimization of Emission Filtering. *Anal. Chem.* **2017**, *89*, 11122−11128.
(13) Gatterdam, V.; Frutiger, A.; Stengele, K.-P.; Heindl, D.; Lübbers, T.; Vörös, J.; Fattinger, C. Focal Molography is a New Method for the In Situ Analysis of Molecular Interactions in Biological Samples. *Nat. Nanotechnol.* **2017**, *12*, 1089−1095.
(14) Krivitsky, V.; Zverzhinetsky, M.; Patolsky, F. Antigen-Dissociation from Antibody-Modified Nanotransistor Sensor Arrays as a Direct Biomarker Detection Method in Unprocessed Biosamples. *Nano Lett.* **2016**, *16*, 6272−6281.
(15) He, X.; Zeng, T.; Li, Z.; Wang, G.; Ma, N. Catalytic Molecular Imaging of MicroRNA in Living Cells by DNA−Programmed Nanoparticle Disassembly. *Angew. Chem., Int. Ed.* **2016**, *55*, 3073−3076.
(16) Xu, L.-P.; Chen, Y.; Yang, G.; Shi, W.; Dai, B.; Li, G.; Cao, Y.; Wen, Y.; Zhang, X.; Wang, S. Ultratrace DNA Detection Based on the Condensing−Enrichment Effect of Superwettable Microchips. *Adv. Mater.* **2015**, *27*, 6878−6884.
(17) Wu, T.-W.; Lee, F.-H.; Gao, R.-C.; Chew, C. Y.; Tan, K.-T. Fluorescent Probe Encapsulated in Avidin Protein to Eliminate Nonspecific Fluorescence and Increase Detection Sensitivity in Blood Serum. *Anal. Chem.* **2016**, *88*, 7873−7877.
(18) Hu, X.; Wang, Y.; Liu, H.; Wang, J.; Tan, Y.; Wang, F.; Yuan, Q.; Tan, W. Naked Eye Detection of Multiple Tumor-related mRNAs from Patients with Photonic-crystal Micropattern Supported Dual-modal Upconversion Bioprobes. *Chem. Sci.* **2017**, *8*, 466−472.
(19) Han, B.; Wang, E. Oligonucleotide-stabilized Fluorescent Silver Nanoclusters for Sensitive Detection of Biothiols in Biological Fluids. *Biosens. Bioelectron.* **2011**, *26*, 2585−2589.
(20) Tang, Y.; Song, H.; Su, Y.; Lv, Y. Turn-on Persistent Luminescence Probe Based on Graphitic Carbon Nitride for Imaging Detection of Biothiols in Biological Fluids. *Anal. Chem.* **2013**, *85*, 11876−11884.
(21) Zhuang, Y.; Xu, Q.; Huang, F.; Gao, P.; Zhao, Z.; Lou, X.; Xia, F. Ratiometric Fluorescent Bioprobe for Highly Reproducible Detection of Telomerase in Bloody Urines of Bladder Cancer Patients. *ACS Sens.* **2016**, *1*, 572−578.
(22) Li, Y.; Gecevicius, M.; Qiu, J. Long Persistent Phosphors−from Fundamentals to Applications. *Chem. Soc. Rev.* **2016**, *45*, 2090−2136.
(23) Wang, Y.; Yang, C.-X.; Yan, X.-P. Hydrothermal and Biomineralization Synthesis of a Dual-modal Nanoprobe for Targeted Near-infrared Persistent Luminescence and Magnetic Resonance Imaging. *Nanoscale* **2017**, *9*, 9049−9055.
(24) Li, Z.; Zhang, Y.; Wu, X.; Huang, L.; Li, D.; Fan, W.; Han, G. Direct Aqueous-Phase Synthesis of Sub-10 nm "Luminous Pearls" with Enhanced in Vivo Renewable Near-Infrared Persistent Luminescence. *J. Am. Chem. Soc.* **2015**, *137*, 5304−5307.
(25) Wang, J.; Ma, Q.; Zheng, W.; Liu, H.; Yin, C.; Wang, F.; Chen, X.; Yuan, Q.; Tan, W. One-Dimensional Luminous Nanorods Featuring Tunable Persistent Luminescence for Autofluorescence-Free Biosensing. *ACS Nano* **2017**, *11*, 8185−8191.
(26) Wang, J.; Ma, Q.; Hu, X.-X.; Liu, H.; Zheng, W.; Chen, X.; Yuan, Q.; Tan, W. Autofluorescence-Free Targeted Tumor Imaging Based on Luminous Nanoparticles with Composition-Dependent Size and Persistent Luminescence. *ACS Nano* **2017**, *11*, 8010−8017.
(27) Chen, L.-J.; Sun, S.-K.; Wang, Y.; Yang, C.-X.; Wu, S.-Q.; Yan, X.-P. Activatable Multifunctional Persistent Luminescence Nanoparticle/Copper Sulfide Nanoprobe for in Vivo Luminescence Imaging-Guided Photothermal Therapy. *ACS Appl. Mater. Interfaces* **2016**, *8*, 32667−32674.
(28) Wang, J.; Ma, Q.; Liu, H.; Wang, Y.; Shen, H.; Hu, X.; Ma, C.; Yuan, Q.; Tan, W. Time-Gated Imaging of Latent Fingerprints and Specific Visualization of Protein Secretions via Molecular Recognition. *Anal. Chem.* **2017**, *89*, 12764−12770.
(29) Zhao, H.-X.; Yang, C.-X.; Yan, X.-P. Fabrication and Bioconjugation of B^{III} and Cr^{III} Co-doped $ZnGa_2O_4$ Persistent Luminescent Nanoparticles for Dual-Targeted Cancer Bioimaging. *Nanoscale* **2016**, *8*, 18987−18994.
(30) Li, N.; Li, Y.; Han, Y.; Pan, W.; Zhang, T.; Tang, B. A Highly Selective and Instantaneous Nanoprobe for Detection and Imaging of Ascorbic Acid in Living Cells and in Vivo. *Anal. Chem.* **2014**, *86*, 3924−3930.
(31) Wu, B.-Y.; Yan, X.-P. Bioconjugated Persistent Luminescence Nanoparticles for Föster Resonance Energy Transfer Immunoassay of Prostate Specific Antigen in Serum and Cell Extracts without in Situ Excitation. *Chem. Commun.* **2015**, *51*, 3903−3906.
(32) Zhang, L.; Lei, J.; Liu, J.; Ma, F.; Ju, H. Persistent luminescence nanoprobe for biosensing and lifetime imaging of cell apoptosis via time-resolved fluorescence resonance energy transfer. *Biomaterials* **2015**, *67*, 323−334.
(33) Chan, E. C. Y.; Pasikanti, K. K.; Hong, Y.; Ho, P. C.; Mahendran, R.; Mani, L. R. N.; Chiong, E.; Esuvaranathan, K. Metabonomic Profiling of Bladder Cancer. *J. Proteome Res.* **2015**, *14*, 587−602.
(34) Lee, Y.; Kischuk, E.; Crist, S.; Ratliff, T. L.; Thompson, D. H. Targeting and Internalization of Liposomes by Bladder Tumor Cells Using a Fibronectin Attachment Protein-Derived Peptide−Lipopolymer Conjugate. *Bioconjugate Chem.* **2017**, *28*, 1481−1490.
(35) Ichimi, T.; Enokida, H.; Okuno, Y.; Kunimoto, R.; Chiyomaru, T.; Kawamoto, K.; Kawahara, K.; Toki, K.; Kawakami, K.; Nishiyama, K.; Tsujimoto, G.; Nakagawa, M.; Seki, N. Identification of Novel MicroRNA Targets based on MicroRNA Signatures in Bladder Cancer. *Int. J. Cancer* **2009**, *125*, 345−352.
(36) Matullo, G.; Naccarati, A.; Pardini, B. MicroRNA Expression Profiling in Bladder Cancer: the Challenge of Next−Generation Sequencing in Tissues and Biofluids. *Int. J. Cancer* **2016**, *138*, 2334−2345.
(37) Hou, J.; Li, M.; Song, Y. Patterned Colloidal Photonic Crystals. *Angew. Chem., Int. Ed.* **2018**, *57*, 2544−2553.
(38) Tan, Y.; Hu, X.; Liu, M.; Liu, X.; Lv, X.; Li, Z.; Wang, J.; Yuan, Q. Simultaneous Visualization and Quantitation of Multiple Steroid Hormones Based on Signal−Amplified Biosensing with Duplex Molecular Recognition. *Chem. - Eur. J.* **2017**, *23*, 10683−10689.
(39) Shen, P.; Li, W.; Liu, Y.; Ding, Z.; Deng, Y.; Zhu, X.; Jin, Y.; Li, Y.; Li, J.; Zheng, T. High-Throughput Low-Background G-Quadruplex Aptamer Chemiluminescence Assay for Ochratoxin A Using a Single Photonic Crystal Microsphere. *Anal. Chem.* **2017**, *89*, 11862−11868.
(40) Du, Y.; Guo, S.; Dong, S.; Wang, E. An Integrated Sensing System for Detection of DNA Using New Parallel-motif DNA Triplex System and Graphene−Mesoporous Silica−Gold Nanoparticle Hybrids. *Biomaterials* **2011**, *32*, 8584−8592.

DOI: 10.1021/acssensors.9b00927
ACS Sens. 2019, 4, 2124−2130